Properties of periodic multicrystal configurations in walk-off-compensating second harmonic generation of ultrashort pulses*

Huang Jin-Zhe(黄金哲)†, Zhang Liu-Yang(张留洋), and Shen Tao(沈 涛)

Department of Optical Information Science and Technology, Harbin University of Science and Technology, Harbin 150080, *China*

(Received 8 June 2010; revised manuscript received 16 October 2010)

This work designs a four-platelet periodic multicrystal configuration in the second harmonic generation of ultrashort pulses as a new walk-off-compensating device. It theoretically investigates a proposed active and a typical passive compensating scheme with the undepleted-pump approximation. The result shows that the angular and spectral bandwidths are proportional to the number of crystal pairs as expected, but the temperature tunability is basically unaltered owing to inter-plate pulse interference. At the same time, an analysis reveals that a misuse of the phase mismatch factor is responsible for a historic controversy about pulse interference. A real design of an ultraviolet second harmonic generation (262.5 nm) is considered in a passive periodic β-Barium Borate-calcite configuration, where the inter-plate pulse interference is found to form an azimuthal tuning restriction and to lower plate length tolerance. A subsequent numerical simulation with pump depletion is in good accordance with theoretical prediction.

Keywords: ultrashort pulses, second harmonic generation, periodic-multicrystal-configurations, walk-off-compensating

PACS: 42.65.Ky, 42.70.Mp, 42.79.Nv **DOI:** 10.1088/1674-1056/20/4/044206

1. Introduction

Frequency up-conversion processes of ultrashort pulses have many potential applications in spectroscopy, optical communications, coherence measurement, etc. Various types of cascaded multi-harmonic generation of ultrashort pulses are often used for different purposes. Second harmonic generation (SHG) is a basic step for cascaded $\chi^{(2)}$ frequency mixing processes. Recent experimental developments further extend its applications.[1−4] Within such an operation, the beam quality of pumping pulses in the space-time domain governs the subsequent output performance. The main reasons for beam quality being degraded and efficiency being lowered in an SHG process were known earlier as spatiotemporal walk-off,[5−7] originating from birefringence and dispersion, respectively. The spatial walk-off vanishes in the known noncritical phase-matching case, in wave guides or can be compensated by periodic-multicrystal-configuration (PMCC).[8−13] Luckily, the spatial walk-off is of the least importance for femtosecond light applications in very short (far less than 1 mm) birefringent crystals, as in the most situations of interest. General group-velocity mismatch (GVMM) or temporal walk-off between the fundamental and the second harmonic waves places a restriction on the birefringent phase-matching process, which incurs conversion falling and pulse width broadening. Zero GVMM appears at retracting points of nonlinear crystals.[14] However, only a very narrow spectral range is available for SHG without GVMM. A classical method is to use spectral angular dispersion (or achromatic phase-matching) by dispersive elements, such as grating or prism pairs,[15−19] to increase spectral bandwidth. In the time domain, the fundamental ultrashort pulses are tilted (wavefront) and focused, which, as Schober *et al.* pointed out,[20] magnify their diffraction. The induced effective dispersion (parameter D) goes far away from confocal focusing, ultimately decreasing the conversion efficiency. Thus a trade-off must be made between the spatial walk-off, crystal length and diffraction loss, accompanied by a complex spectral technique: a precise spatiotemporal chirp compensation through dispersive elements. In 1998, Smith *et al.*[10] presented a novel idea of a passive walk-off-compensating (WOC) scheme by the PMCC, which was implemented later by making use of five programmed β-Barium Borate

*Project supported by the Tiptop-Talent Fund from Harbin University of Science and Technology.

†Corresponding author. E-mail: huangjinzhe@hrbust.edu.cn

© 2011 Chinese Physical Society and IOP Publishing Ltd

(β-BBO or BBO) segments to generate blue femtosecond pulses.[11] The principle of GVMM compensation in SHG was also used by Huang *et al.* in quasi-phase matched waveguide elements using bent fibres,[21] by Fülöp *et al.* through a prism pair in a single crystal,[22] and by Sapaev and Assanto for picosecond pulses via frequency-selective mirrors,[23] which was also extended to a sum frequency generation.[24,25] The PMCC lengthens the coupling process, increases the phase-matching bandwidth and compresses the spatiotemporal walk-off in comparison with a single bulk nonlinear crystal, as is roughly predicted by Smith *et al.* It is then more attractive for the frequency conversion of low power ultrashort pulse lasers. However, there is a contradiction between the theoretical results of long-pulse SHG delivered by different literature. In a well-compensated case, some researchers claimed the existence of an interference factor (or filter function)[12,13,26] in the expression of output field intensity but others did not.[9,10,27–29] In 2003, Pack *et al.* noticed this problem and argued against the factor with some carefully chosen experiments.[29] But in the same year, Zondy *et al.* upheld its existence through a theoretical deduction, also with experiments.[12,13] Thus it seems necessary to ascertain the truth in the dispute, so as to assure the validity of the modeling here. In this study, an effective heuristic approach is adopted for presenting wave propagation and interference, and our attention is focused on the tuning properties of a PMCC in the ultrashort pulse SHG.

2. Model and method

2.1. The SHG in a PMCC

We recommend a WOC PMCC, compensating the spatiotemporal walk-off, which requires four platelets in use as a unit. Figure 1 illustrates a typical PMCC, which is nearly the same as the one that Smith *et al.*[10] used, except that they only installed two platelets in one unit. There are two kinds of alternate crystal segments ($4N$). One is the generating crystal (GC) mainly for SHG, as the active one; the other is the compensating crystal (CC) serving for GVMM compensation, as the passive one. There is another possibility that the CC can also act as a secondary SHG source, forming an active WOC scheme, which is detailed in the appendix, and will be considered in the following development. One GC and one successive CC constitute one pair, and four segments build one unit, where the spatial walk-off in identical crystal pairs (GC_1–GC_2 and CC_1–CC_2), and temporal walk-off in different crystal pairs (GC_1–CC_1 and GC_2–CC_2) are compensated for. This differs from the multicrystal structure designed by Brown, aiming at broadening the spectral bandwidth,[30] where each nonlinear crystal plate converts a portion of the spectrum of fundamental pulses, at a cost of conversion reduction. The GCs and CCs are simply taken as uniaxial crystals with lengths of l_1 and l_2, respectively, and the pumping pulses are assumed to be free of diffraction and spatiotemporal chirp. The last CC in Fig. 1 is only for a fluent theoretical treatment, and certainly is not necessary in an application. The PMCC can be designed as a folded geometry in light paths, as it only needs four platelets in total. One may doubt this four-platelet PMCC by pointing out that one CC is enough to compensate for the spatiotemporal walk-off, as that in Ref. [11]. Actually, the simplified two-platelet structure endures a bad angular tunability, which will be shown later.

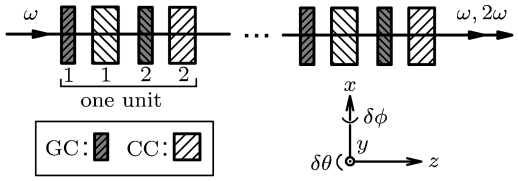


Fig. 1. PMCC design for GVMM compensated SHG. The shadowed directions schematically denote relevant optic axes.

The simple undepleted-pump approximation is adequate to develop the tuning characteristics of PMCC. Concretely, the type I SHG in the j-th pair follows the well-known time-dependent (τ) equation

$$\frac{\partial A_{j\mu}^{(2)}}{\partial z} + \frac{1}{u_\mu^{(2)}}\frac{\partial A_{j\mu}^{(2)}}{\partial \tau} + \rho_{j\mu}\frac{\partial A_{j\mu}^{(2)}}{\partial x} + \frac{\mathrm{i}\,\beta_\mu^{(2)}}{2}\frac{\partial^2 A_{j\mu}^{(2)}}{\partial \tau^2} = \mathrm{i}\,\sigma_\mu A_{j\mu}^{(1)2}\exp(\mathrm{i}\,\Delta k_{j\mu} z), \quad (1)$$

where absorption terms are neglected since the total length is relatively small, μ=1 for GC and 2 for CC; z, the coordinate in the propagating direction (every plate has its own z coordinate with an associated origin on its incident surface); x, a mutual transverse coordinate in all plates, as well as y (omitted here); $\Delta k_{j\mu} = 2k_{j\mu}^{(1)} - k_{j\mu}^{(2)}$, the known wave constant mismatches between the pulses whose central wavelengths are λ_1, λ_2; σ_μ, the coupling parameters proportional to the second order effective susceptibilities in GCs and CCs (if active); $\rho_{j\mu}$, the tangent values of the walk-off angles between the harmonic and fundamental beams; $u_\mu^{(1)}$, $u_\mu^{(2)}$, the group-velocities, which are

independent of j owing to the alternation of crystal plates; $\beta_\mu^{(1)}$, $\beta_\mu^{(2)}$ are the coefficients of group-velocity dispersion, responsible for pulse broadening. However the broadening is weak over several units in a PMCC, so they are reasonably neglected except for a rigorous simulation, which is carried out in Section 4. The amplitudes of the fundamental and harmonic pulses have the forms of traveling waves $A_{j\mu}^{(1)}(x,\zeta,\tau-z/u_\mu^{(1)})$, $A_{j\mu}^{(2)}(x,\zeta,\tau-z/u_\mu^{(2)})$ with $\zeta=z$ (ζ will be neglected below for conciseness). They are connected to real fields by

$$\boldsymbol{E}_{j\mu}^{(\nu)}=\frac{1}{2}\hat{\boldsymbol{e}}_\nu A_{j\mu}^{(\nu)}\exp[\mathrm{i}(k_{j\mu}^{(\nu)}z-\omega_\nu\tau)]+\text{c.c.}, \quad (2)$$

for $\nu=1,2$ with the unit vectors $\hat{\boldsymbol{e}}_\nu$, wave constants $k_{j\mu}^{(\nu)}$, angular frequencies ω_ν which correspond to the central wavelengths λ_ν. All crystal plates will generate similar harmonic pulses through interactions, but own alternate amplitudes and phases. During the pulse interactions, the phase mismatch in previous stages will accumulate forwardly, with which one should deal carefully. Actually only the relative phase difference between a harmonic pulse and its driving polarization field needs to be taken. When a generated harmonic pulse is in phase with its driving source (the nonlinear polarization field $P^{(2)}\propto E^{(1)2}$) before reaching the $(j\mu)$-th plate, the harmonic pulse will catch a retarded phase $\Delta k_{j\mu}l_\mu$ just after passing it. This reasoning is confirmed in Section 3. In an analogous way, the harmonic pulse has a spatial walk-off magnitude $\rho_{j\mu}l_\mu$ towards the x direction, and has a temporal walk-off $\delta u_\mu l_\mu$ induced by the $(j\mu)$-th plate, where the inverse GVMM $\delta u=1/u^{(2)}-1/u^{(1)}$ is used to describe the temporal walk-off. Then, by a straightforward calculation, if a harmonic pulse propagates from the $(j\mu)$-th to the last plate, then it will have a total lagging phase $p_{j\mu}$, and a total spatial and temporal walk-off $x_{j\mu}$, $t_{j\mu}$, respectively, i.e.,

$$p_{j\mu}=-\Delta k_{j1}l_1\delta_{2\mu}+\sum_{m=j}^{2N}(\Delta k_{m1}l_1+\Delta k_{m2}l_2), \quad (3a)$$

$$x_{j\mu}=-\rho_{j1}l_1\delta_{2\mu}+\sum_{m=j}^{2N}(\rho_{m1}l_1+\rho_{m2}l_2), \quad (3b)$$

$$t_{j\mu}=-\delta u_1 l_1\delta_{2\mu}+(2N-j+1)(\delta u_1 l_1+\delta u_2 l_2). \quad (3c)$$

Here the dispersion of air and Fresnel reflection losses are simply omitted. The kronecker symbol $\delta_{2\mu}$ is nonvanishing (=1) only at μ=2. Thus by Eqs. (1) and (3), the amplitude addition of the j-th harmonic pulse pair in air is

$$A_j^{(2)}=\mathrm{i}\sum_{\mu=1}^{2}\frac{\sigma_\mu}{\sqrt{n_\mu}}\int_0^{l_\mu}\bar{A}_{j\mu}^2\exp[\mathrm{i}(\Delta k_{j\mu}z-p_{j\mu})]\mathrm{d}z, \quad (4a)$$

$$\bar{A}_{j\mu}\triangleq\sqrt{n_\mu}A_{j\mu}^{(1)}(x-x_{j\mu}+\rho_{j\mu}z,t-t_{j\mu}+\delta u_\mu z), \quad (4b)$$

$$t\triangleq\tau-2j\sum_{\nu=1}^{2}l_\nu/u_\nu^{(1)}+l_1\delta_{2\mu}/u_1^{(1)}-z/u_\mu^{(1)}, \quad (4c)$$

where t is the local time, which is a time coordinate relative to the driving fundamental pulses where the time consuming in air is not counted in. The n_μ are the refractive indices that satisfy the type-I phase-matching condition. The $\bar{A}_{j\mu}$ are the fundamental field amplitudes in air. $\bar{A}_{j\mu}^2$, in proportion to the harmonic amplitudes generated at the source spatiotemporal location ($x-x_{j\mu}+\rho_{j\mu}z$, z, $t-t_{j\mu}+\delta u_\mu z$), are described at the observation position (x, $z=l_2$, t) on the exit surface of the last plate. The relationship between the source and observation positions can be obtained by a heuristic approach to the light rays' propagation. The total harmonic pulse is then a superposition of Eq. (4a) from all N units.

Equations (3) and definition (4b) show a uniform formulation among the spatial, temporal walk-offs and the phase lag. This formal analog implies that possibly there are similar compensation methods by consecutively reversing walk-off parameters. From Eq. (3b), it can be seen that the periodically reversed spatial walk-offs $\rho_{j\mu}=-\rho_{(j+1)\mu}$ suppress the total walk-off distance to a magnitude no more than $|\rho_{11}l_1+\rho_{12}l_2|$. Provided that a CC compensates a GC for its GVMM, the following condition must be satisfied:

$$\delta u_1 l_1+\delta u_2 l_2=0. \quad (5)$$

This means that a retarded harmonic pulse after a GC will be advanced by passing a followed CC, so that the fundamental and harmonic pulses can be synchronized with a coincidence of the centroids of their pulse envelopes. Moreover, the sign of $\delta u_1/\delta u_2$ must be negative, which is a primary requirement, and l_1, l_2 should be restricted by the temporal walk-off in the GC and CC (if active), respectively, i.e., $|\delta u_\mu l_\mu|\leqslant\Delta\tau$, where $\Delta\tau$ is the duration of the fundamental pulses with respect to the full width at half maximum (it is also accepted here to estimate angular widths).

2.2. Angular tuning in an active PMCC

First, we consider an active PMCC under an angular detuning. Letting $\theta_{j\mu}$ be the angles of optic axes with respect to the z axis in the range $(-\pi/2,\pi/2]$, we find that the alternation of the optic axes [Fig. 1(a)] renders $\theta_{j\mu}=(-1)^{j+1}\theta_\mu$, where θ_μ are the angles in the first crystal pair. Then a variation $\delta\theta$ of the

external angle of incidence causes the internal angular tilts $\delta\theta_{j\mu}$. The wave constant mismatches on the condition of critical phase-matching vary with $\theta_{j\mu}$ as $\Delta k_{j\mu} \propto \delta\theta_{j\mu} = (-1)^{j+1}\delta\theta_{\mu}$. So a tilted incident light leads to a periodic reverse of mismatches

$$\Delta k_{j\mu} = (-1)^{j+1}\Delta k_{1\mu}. \tag{6}$$

It will be shown below that the very reverse of the wave constant mismatches decreases walk-off times or broadens acceptance bandwidths. With Eq. (5), $\Delta t_{j\mu} = \Delta t_{\mu} = \delta_{2\mu}\delta u_2 l_2$ are independent of j by Eq. (3c), and if the spatial walk-off $\rho_{j\mu}$ is neglected, $\bar{A}_{j\mu}$ can be simplified as $\bar{A}_{\mu}$. Then the integration in Eq. (4a) can be rewritten as

$$\begin{aligned}&\int_0^{l_\mu} \bar{A}_\mu^2 \exp(\mathrm{i}\,\Delta k_{j\mu} z)\mathrm{d}z \\ &= \exp(\mathrm{i}\,\Gamma_{j\mu}) \int_{-l_\mu/2}^{l_\mu/2} \bar{A}_\mu^2(t' + \delta u_\mu z_\mu) \\ &\quad \times \exp(\mathrm{i}\,\Delta k_{j\mu} z_\mu)\mathrm{d}z_\mu \\ &= \exp[\mathrm{i}(\Gamma_{j\mu} + \alpha_{j\mu})] l_\mu B_\mu(t')\end{aligned} \tag{7}$$

with $z_\mu = z - l_\mu/2$, $t' = t + \delta u_1 l_1/2$ and

$$B_\mu \triangleq \frac{1}{l_\mu}\int_{-l_\mu/2}^{l_\mu/2} \bar{A}_\mu^2(t' + \delta u_\mu z_\mu)\mathrm{d}z_\mu, \tag{8a}$$

$$\Gamma_{j\mu} \triangleq \Delta k_{j\mu} l_\mu/2, \tag{8b}$$

where $\Gamma_{j\mu}$ are the phase mismatch parameters, $\alpha_{j\mu}(t', \Gamma_{j\mu}) = \alpha'_{j\mu} + \mathrm{i}\,\alpha''_{j\mu}$, whose components $\alpha'_{j\mu}$, $\alpha''_{j\mu}$ are real functions. The $\alpha'_{j\mu}$ represent the strengths of phase modulation, and $\alpha''_{j\mu}$ indicate the dephasing effect due to phase mismatch. Here, $\exp(\mathrm{i}\,\alpha_{j\mu})$ are some formal solutions that cannot be expressed analytically. With $|\delta u_\mu l_\mu|/\Delta\tau$ approaching zero, there are the tendencies: $\alpha'_{j\mu} \to 0$, $\exp(-\alpha''_{j\mu}) \to \mathrm{sinc}(\Gamma_{j\mu})$. However, experimentally, these limits can hardly be satisfied for femtosecond pulses except in a very thin plate whose length is far less than a characteristic temporal walk-off length, so a remarkable walk-off up to $|\delta u_\mu l_\mu| \sim \Delta\tau$ has to be considered. For example, a Gaussian form of fundamental pulses will make B_μ an error function, while $B_\mu \exp(\mathrm{i}\,\alpha_{j\mu})$ is a complex error function. The reason we choose a symbolic form of $\alpha_{j\mu}$ is to better transfer the tuning effect in this paper. For the chirp-free real amplitudes $\bar{A}_\mu$, a conjugation of Eq. (7) is equivalent to a replacement: $\Delta k_{j\mu} \to -\Delta k_{j\mu}$. It makes $\alpha'_{j\mu}$ odd and $\alpha''_{j\mu}$ even functions of $\Delta k_{j\mu}$ (or $\Gamma_{j\mu}$). Equation (6) infers that

$$\alpha'_{j\mu} = (-1)^{j+1}\alpha'_{1\mu}, \alpha''_{j\mu} = \alpha''_{1\mu}. \tag{9}$$

In the following paragraphs, the subscript "1μ" will be simplified as "μ", as it does not cause an ambiguity. Then through Eqs. (3a), (4a), (6) and (9), the total harmonic pulse amplitude can be written as a resultant of the complex phasor amplitudes from GCs and CCs, i.e.,

$$\begin{aligned}A_2 &= \sum_{j=1}^{2N} A_j^{(2)} = \mathrm{i}\sum_{\mu=1}^{2} \bar{\sigma}_\mu B_\mu \exp(-\alpha''_\mu) \\ &\quad \times \sum_{j=1}^{2N} \exp[\mathrm{i}(\Gamma_{j\mu} + \alpha'_{j\mu} - \Delta p_{j\mu})] \\ &= \mathrm{i}\,2N \sum_{\mu=1}^{2} \bar{\sigma}_\mu B_\mu \exp[\mathrm{i}(\Gamma_1 + \Gamma_2) - \alpha''_\mu] \\ &\quad \times \cos(\Gamma'_{\bar{\mu}}),\end{aligned} \tag{10}$$

where $\bar{\mu} = 3 - \mu$, $\Gamma'_\mu \triangleq \Gamma_\mu - (-1)^\mu \alpha'_{\bar{\mu}}$, $\bar{\sigma}_\mu \triangleq \sigma_\mu l_\mu n_\mu^{-1/2}$ and the losses due to Fresnel reflections are neglected too. The term $\cos(\Gamma'_{\bar{\mu}})$ or $\cos(\Gamma_{\bar{\mu}})$, reflects the interference between harmonic pulses in a unit, which is then termed intra-unit pulse interference here.

The pulse dephasing function, which is commonly used to demonstrate the tuning characteristic, can be defined by the ratio of the energy density of a phase mismatched harmonic pulse to that of a phase matched one. For this purpose, it is useful to define the following matrix functions,

$$\begin{aligned}D_X^{\mu\nu} &\triangleq \frac{\bar{\sigma}_\mu \bar{\sigma}_\nu}{P}\int_{-\infty}^{\infty} B_\mu B_\nu^* \exp(-\alpha''_\mu - \alpha''_\nu) \\ &\quad \times g_1(\alpha'_\mu) g_2(\alpha'_\nu)\mathrm{d}t',\end{aligned} \tag{11}$$

where $g_{1,2}$ are the cosine or sine functions. We may label the subscript X as c for $g_{1,2}$=cos, as s for $g_{1,2}$=sine, as m for g_1=cos and g_2=sine. Then we have the cosine, sine and cosine–sine mixed dephasing coefficients with μ, ν=1,2 and

$$P \triangleq \int_{-\infty}^{\infty} |\bar{\sigma}_1 B_1 + \bar{\sigma}_2 B_2|^2 \,\mathrm{d}t' \tag{12}$$

is the pulse energy density (by a constant) under a perfect phase-matching condition. Note that $B_{1,2}$ and $\alpha_{1,2}$ are the functions of t' according to Eqs. (7), and (8), and $B_1 = B_2$ if the GVMM is well compensated. The dephasing matrix represents the phase mismatch effect of SHG in just one pair of GC+CC and the interference between the two harmonic pulses generated from them. Equation (11) is suitable for an arbitrary temporal walk-off. Furthermore, by defining the cosine and sine vectors as

$$\boldsymbol{S}_c^{\mathrm{t}} \triangleq (\cos\Gamma_2, \cos\Gamma_1), \tag{13a}$$

$$\boldsymbol{S}_s^{\mathrm{t}} \triangleq (\sin\Gamma_2, -\sin\Gamma_1), \tag{13b}$$

where the superscript "t" means a transpose, the pulse dephasing function according to the previous definition becomes

$$\begin{aligned} D_a &\triangleq \frac{\int_{-\infty}^{\infty}|A_2|^2\mathrm{d}t'}{\int_{-\infty}^{\infty}|A_2(\Delta k_{j\mu}=0)|^2\mathrm{d}t'} \\ &= \boldsymbol{S}_c^{\mathrm{t}}\cdot\boldsymbol{D}_c\cdot\boldsymbol{S}_c+\boldsymbol{S}_s^{\mathrm{t}}\cdot\boldsymbol{D}_s\cdot\boldsymbol{S}_s \\ &\quad +2\boldsymbol{S}_c^{\mathrm{t}}\cdot\boldsymbol{D}_m\cdot\boldsymbol{S}_s. \end{aligned} \tag{14}$$

Accordingly, the pulse energy density is $c\epsilon_0 PD_a/2$, where ϵ_0 is the permittivity in free space. Other dephasing functions will follow the same definition as the first line in Eq. (14). The total dephasing effect can be decomposed into a combination of the basic dephasing effect within one pair configuration and the intra-unit pulse interference in a quadratic form. This gives the pattern of the pulse coherence affects the dephasing processes. The diagonal cosine and sine dephasing coefficients $D_c^{\mu\mu}$, $D_s^{\mu\mu}$ for Gaussian fundamental pulses are shown in Fig. 2, where μ=1 or 2.

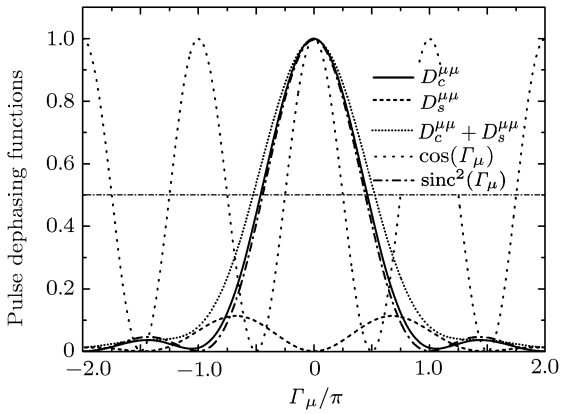


Fig. 2. Diagonal cosine ($D_c^{\mu\mu}$) and sine ($D_s^{\mu\mu}$) dephasing coefficients together with the dephasing function of a single nonlinear crystal ($D_c^{\mu\mu}+D_s^{\mu\mu}$), all of which are divided by $D_c^{\mu\mu}$ (Γ_μ=0), and an approximate dephasing function $\mathrm{sinc}^2(\Gamma_\mu)$ with the interference factor $\cos^2(\Gamma_\mu)$ in a critical walk-off case $|\delta u_\mu l_\mu| = \Delta\tau$.

It is found that the cardinal-sine-squared function $\mathrm{sinc}^2(\Gamma_\mu)$ is a good approximation to $D_c^{\mu\mu}$, and $D_s^{\mu\mu}$ can be approximated by a squared first order spherical bessel function $\mathrm{j}_1^2(\cdot)$, i.e.,

$$D_c^{\mu\mu}\approx\left(\frac{\bar\sigma_\mu}{\bar\sigma_1+\bar\sigma_2}\right)^2\mathrm{sinc}^2(\Gamma_\mu), \tag{15a}$$

$$D_s^{\mu\mu}\approx 0.32\left[\frac{\delta u_\mu l_\mu\bar\sigma_\mu}{\Delta\tau(\bar\sigma_1+\bar\sigma_2)}\right]^2\mathrm{j}_1^2(\Gamma_\mu). \tag{15b}$$

Relations (15a) and (15b) can be used for a quantitative estimation within $|\delta u_\mu l_\mu|\leqslant\Delta\tau$. In a single nonlinear plate, the dephasing function becomes a simple summation $D_c^{\mu\mu}+D_s^{\mu\mu}$. Because $\boldsymbol{D}_s$ (sometimes even $\boldsymbol{D}_m$) is much less than $\boldsymbol{D}_c$, it is ignorable when the sine vector $\boldsymbol{S}_s$ is small enough within the main peak of $\boldsymbol{D}_c$, and the cosine approximation will simplify a real calculation. Furthermore, if $\bar A_{j\mu}$ is an even function of t', e.g. the Gaussian pulse shape, from the second integrand in Eq. (7), it can be proved that the time reversal $t'\to -t'$ can be substituted with the reversal of wave constant mismatch $\Delta k_{j\mu}\to-\Delta k_{j\mu}$. Then α'_μ, α''_μ are odd and even functions of t' respectively. Therefore $\boldsymbol{D}_m$=0. Calculations are then simplified further.

Since the pulse dephasing function D_a is irrelevant to N, the angular bandwidth in an active WOC PMCC is equal to that of one pair configuration. So, the bandwidth is a combined result of a GC plus a CC and just weakly depends on $\bar\sigma_{1,2}$. Taking the cosine approximation with a symmetrical fundamental wave form leads to $D_a\approx\boldsymbol{S}_c^{\mathrm{t}}\cdot\boldsymbol{D}_c\cdot\boldsymbol{S}_c$.

2.3. Angular tuning in a passive PMCC

In a passive case $\bar\sigma_2=0$, Γ_{j2} are far from zero. According to Eq. (10), achieving a maximal output requires Γ_1=0 and $\Gamma_2=m\pi$ ($m\in\mathbb{Z}$ is generally not small). It makes an analysis of the angular bandwidth a subtle issue. Under an angular tilt, the derivation of A_2 should be reconsidered. It has to be emphasized that $|\Delta k_{j2}|$ may go far greater than π/l_2, therefore a small variation in the passing length in a CC might cause an appreciable phase mismatch. That fails to form the periodic wave constant mismatches in CCs, and there are

$$\Delta k_{j1}=(-1)^{j+1}\Delta k_{11},\quad \Delta k_{j2}=\Delta k_{(j+2)2}. \tag{16}$$

With the definitions

$$\psi\triangleq\Gamma_{12}+\Gamma_{22}, \tag{17a}$$

$$f_N(\psi)\triangleq\sin(N\psi)/[N\sin(\psi)], \tag{17b}$$

the output harmonic pulse becomes

$$\begin{aligned} A_2 &= \sum_{j=1}^{2N}A_j^{(2)}=\mathrm{i}\,\bar\sigma_1 B_1\exp(-\alpha''_1) \\ &\quad\times\sum_{j=1}^{2N}\exp[\mathrm{i}(\Gamma_{j1}+\alpha'_{j1}-p_{j1})] \\ &= \mathrm{i}\exp[\mathrm{i}(\Gamma_1-\Gamma_{22}-N\psi)-\alpha''_1] \\ &\quad\times 2N\bar\sigma_1 B_1\cos(\Gamma'_2)f_N(\psi), \end{aligned} \tag{18}$$

where the emergence of $f_N(\psi)$ shows a coherence of N harmonic pulses generated from the odd or even crystal pairs in different units, whose square is just the normalized interference function in the Fraunhofer

theory of diffraction gratings, where it is called the inter-unit pulse interference factor. It also appears in a two-platelet WOC configuration incurring an imperfect compensation for the phase mismatch.[27] The last line in Eq. (18) is just a combination of the intra- and inter-unit pulse interferences, as it is referred to as inter-plate pulse interference here. The pulse dephasing function, indicated by D_p, can be expressed as Eq. (14) multiplying the inter-unit pulse interference factor at $\bar{\sigma}_2 = 0$, i.e.,

$$\begin{aligned} D_p &= (\boldsymbol{S}_c^{\mathrm{t}} \cdot \boldsymbol{D}_c \cdot \boldsymbol{S}_c + \boldsymbol{S}_s^{\mathrm{t}} \cdot \boldsymbol{D}_s \cdot \boldsymbol{S}_s \\ &\quad + 2\boldsymbol{S}_c^{\mathrm{t}} \cdot \boldsymbol{D}_m \cdot \boldsymbol{S}_s) f_N^2(\psi) \\ &= [D_c^{11} \cos^2(\Gamma_2) + D_s^{11} \sin^2(\Gamma_2) \\ &\quad + \sin(2\Gamma_2) D_m^{11}] f_N^2(\psi), \end{aligned} \tag{19}$$

with the pulse energy density $c\epsilon_0 P D_p/2$. Under the cosine approximation, it becomes

$$D_p \approx \mathrm{sinc}^2(\Gamma_1) \cos^2(\Gamma_2) f_N^2(\psi). \tag{20}$$

The inter-plate pulse interference brings a close restriction on angular bandwidths at worst. In a design of PMCC, fortunately, it is possible to make Γ_{12}, Γ_{22} cancel with each other to a certain extent, which will weaken the impact of the interference so as to broaden the bandwidths. This is the main reason why the four-platelet PMCC is preferred.

2.4. Spectral and temperature tunings

As other tunable parameters are concerned, the resulting amplitudes differ in the way of interference. In both the active and passive WOC methods, equation (5) and the second equation in Eqs. (A1) lead to the following conditions,

$$\Delta k_{j1} l_1 = -\Delta k_{j2} l_2, \quad \Delta k_{(j+1)\mu} = \Delta k_{j\mu}, \tag{21}$$

if a wavelength detune $\delta\lambda$ happens. The Δk_{j2} induced by $\delta\lambda$ is only a portion of a total wave constant mismatch (commonly is $\Delta k_{j2} + 2m_j\pi/l_2$, where m_j is a nonzero integer) in CC_j for the passive compensation. The first equation in Eqs. (21) is derived by the compensation condition (5), which makes a total lagging phase just a number of 2π. So there is a relation $p_{j\mu} = 2\Gamma_1 \delta_{2\mu}$. Following an analogous mathematical procedure in Eq. (10), we find that the amplitude of the output harmonic pulse becomes

$$\begin{aligned} A_2 &= \mathrm{i}\, 2N \sum_{\mu=1}^{2} \exp[\mathrm{i}(\Gamma_\mu + \alpha'_\mu + 2\Gamma_1 \delta_{2\mu})] \\ &\quad \times \bar{\sigma}_\mu B_\mu \exp(-\alpha''_\mu), \end{aligned} \tag{22}$$

where α is regulated as

$$\alpha'_{j\mu} = \alpha'_{1\mu}, \quad \alpha''_{j\mu} = \alpha''_{1\mu}. \tag{23}$$

Equation (22) indicates an ideal coherence of a harmonic pulse train. The total spectral dephasing width is the same as that of one GC in a passive WOC configuration, or that of GC+CC in an active one, as expected. The pulse dephasing function at last is a summation of all components of the cosine and sine dephasing coefficients, i.e.,

$$D_\lambda = D_c^{11} + D_c^{22} + D_s^{11} + D_s^{22} + 2(D_c^{12} + D_s^{12}). \tag{24}$$

It is well understood by Eqs. (21) and (A1) that the temporal walk-off compensation directly leads to the spectral bandwidth broadening.

A temperature detune δT from $T = T_0$ does not bring on any compensation for induced phase mismatch, so only the second equation in Eq. (21) holds. The Δk_{j2} is also a portion of the total wave constant mismatch in CC_j of a passive compensation. The wave constant mismatches are then irrelevant to the periodic inversion of polar angles. Thus, it yields

$$\begin{aligned} A_2 &= \mathrm{i}\, 2N \sum_{\mu=1}^{2} \bar{\sigma}_\mu B_\mu \exp(\mathrm{i}\,\alpha'_\mu - \alpha''_\mu) f_{2N}(\Gamma_1 + \Gamma_2) \\ &\quad \times \exp\{\mathrm{i}[\Gamma_\mu + 2\Gamma_1 \delta_{2\mu} - (2N+1)(\Gamma_1 + \Gamma_2)]\}. \end{aligned} \tag{25}$$

When δT is small enough, a loose estimation

$$\begin{aligned} \exp(-\alpha''_\mu) f_{2N}(\Gamma_1 + \Gamma_2) &\sim \mathrm{sinc}(\Gamma_\mu) f_{2N}(\Gamma_1 + \Gamma_2) \\ &\sim \mathrm{sinc}[2N(\Gamma_1 + \Gamma_2)] \end{aligned} \tag{26}$$

holds. The temperature bandwidth of the PMCC is a mixed effect of the $L_1 = 2Nl_1$ thick GC and the $L_2 = 2Nl_2$ thick CC, or equivalently one bulk GC with a reduced length $L_1 + \Gamma_2 L_2/\Gamma_1$. By defining a vector of complex triangle function $\boldsymbol{S} = \boldsymbol{S}_c + \mathrm{i}\,\boldsymbol{S}_s$, the temperature dephasing function can be written as

$$\begin{aligned} D_T &= [\boldsymbol{S}^\dagger \cdot (\boldsymbol{D}_c + \boldsymbol{D}_s - \mathrm{i}\,\boldsymbol{D}_m + \mathrm{i}\,\boldsymbol{D}_m^{\mathrm{t}}) \cdot \boldsymbol{S}] \\ &\quad \times f_{2N}^2(\Gamma_1 + \Gamma_2) \\ &= f_{2N}^2(\Gamma_1 + \Gamma_2)[D_c^{11} + D_c^{22} + D_s^{11} + D_s^{22} \\ &\quad + 2(D_c^{12} + D_s^{12}) \cos(\Gamma_1 + \Gamma_2) \\ &\quad - 2(D_m^{12} - D_m^{21}) \sin(\Gamma_1 + \Gamma_2)], \end{aligned} \tag{27}$$

where "†" denotes a conjugate transpose.

If an odd number of crystal pairs $2N-1$ is chosen, the expressions are a little different from those above. However, it does not bring new physical phenomena caused by the pair number. So we simply omit it.

3. Controversy

The controversy pertains to the interference in multicrystal configuration. The problem therein can be simply shown by introducing a two-crystal WOC structure (a simple PMCC), as shown in Fig. 3 for SHG of a cw laser.

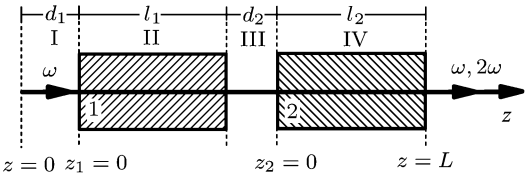


Fig. 3. The typical WOC two-crystal structure for a cw laser SHG, which makes four regions: I, II, III, IV with two relative coordinates: $z_1 = z - d_1$, $z_2 = z - d_1 - d_2 - l_1$. The shadowed directions schematically denote relevant optic axes.

Permitting an arbitrary longitudinal orientation with the origin of the z coordinate outside the first crystal, the propagation space is divided into four regions from I to IV. Due to the spatial nonuniformity, the wave constants for the frequencies ω and 2ω have a stepped form: $K_m = k_{m0}$, k_{m1}, k_{m0}, k_{m2} in the I–IV regions, respectively, where m=1, 2 are for the possible ordinary and extraordinary fundamental waves ($K_1 \neq K_2$ for type II, $K_1 = K_2$ for type I) and m=3 for the harmonic wave. Moreover, for the second subscript index n in k_{mn}, "0" for air, "1" for the first crystal and "2" for the second one. The three waves are made in phase at z=0. Thus, the phase factors of the two coupling plane waves will be

$$\begin{aligned} p_m(z) &= \int_0^z K_m(z')\mathrm{d}z' \\ &= \begin{cases} k_{m0}z, & \text{I}, \\ k_{m0}d_1 + k_{m1}z_1, & \text{II}, \\ k_{m0}d_1 + k_{m1}l_1 + k_{m0}(z - d_1 - l_1), & \text{III}, \\ k_{m0}d_1 + k_{m1}l_1 + k_{m0}d_2 + k_{m2}z_2, & \text{IV}. \end{cases} \end{aligned} \tag{28}$$

Accordingly, the phase mismatch in the nonlinear regions becomes

$$\Delta p(z) = \begin{cases} \Delta k_0 d_1 + \Delta k_1 z_1, & \text{II}, \\ \Delta k_0(d_1 + d_2) + \Delta k_1 l_1 + \Delta k_2 z_2, & \text{IV}, \end{cases} \tag{29}$$

where $\Delta p = p_1 + p_2 - p_3$ ($p_1 = p_2$ for type I) and Δk_0, Δk_1, Δk_2 denote the wave constant mismatches in the I (III), II, IV regions, respectively. The factor Δkz in the well-known coupling equation should be replaced by $\Delta p(z)$, which is believed to be the crux of the controversy. The amplitude of the harmonic wave in the undepleted-pump approximation as such can be written as

$$\begin{aligned} A_2 &= \mathrm{i}\,\sigma \int_{\text{II+IV}} A_1^2 \exp[\mathrm{i}\,\Delta p(z)]\mathrm{d}z \\ &= \{l_1 \mathrm{sinc}(\varphi_1) + \exp[\mathrm{i}(\varphi_0 + \varphi_1 + \varphi_2)] \\ &\quad \times\ l_2 \mathrm{sinc}(\varphi_2)\}\,\mathrm{i}\,\sigma \exp[\mathrm{i}(\varphi_0' + \varphi_1)], \end{aligned} \tag{30}$$

where $\varphi_0' = \Delta k_0 d_1$, $\varphi_0 = \Delta k_0 d_2$, $\varphi_m = \Delta k_m l_m/2$ with m = 1, 2 and φ_0', φ_0 are allowed to include the induced phase mismatches by crystal coatings. Equation (30) directly leads to the harmonic wave intensity

$$\begin{aligned} I_2 \propto\ & \sigma^2[\mathrm{sinc}^2(\varphi_1)l_1^2 + \mathrm{sinc}^2(\varphi_1)l_2^2 \\ &+\ 2l_1 l_2 \cos(\varphi_0 + \varphi_1 + \varphi_2)\mathrm{sinc}(\varphi_1)\mathrm{sinc}(\varphi_2)]. \end{aligned} \tag{31}$$

If a simplified compensating condition φ_0=0, $\varphi_1 + \varphi_2$=0 is met with $l_1 = l_2$, equation (30) yields $A_2 \propto 2\,\mathrm{i}\,\sigma l_1 \mathrm{sinc}(\varphi_1)$, $I_2 \propto 4(\sigma l_1)^2 \mathrm{sinc}^2(\varphi_1)$. When the phase mismatch $\Delta p(z)$ is misinterpreted as Δkz, the light intensity will depend on the location of the origin, which physically does not stand to reason. For example, a conclusion of $I_2 \propto 4(\sigma l_1)^2 \mathrm{sinc}^2(\varphi_1)\cos^2(2\varphi_1)$ was drawn by Fève and Zondy *et al.* with an orientation d_1=0;[12,26] while the same result as Eq. (31) was obtained with a symmetric orientation $d_1 = -l_1$ by coincidence.[29] The interference function $\cos(\Gamma_{\bar{\mu}}')$ appearing in Section 2 is in fact a sign of the four-platelet configuration, which, however, disappears in a two-platelet case, as shown above.

Equation (29) infers that $\Delta p(z)$ is just an accumulated phase mismatch from the origin to the field point z, as up to date is not well clarified in the relevant literature. In addition, $\Delta p(z)$ can be taken as the advanced phase of the driving polarization wave according to the harmonic wave. Alternatively, there is an equivalent heuristic approach, in which case the in-phase position is made at the exit surface of the last crystal, the observation position. Then the advanced phase of the driving polarization wave at z turns into $\Delta p(z) - \Delta p(L)$, which otherwise can be taken as the retarded phase of the generated harmonic wave with respect to the driving source. This heuristic approach is adopted in the model section of this paper [equation (3a) is a form of $\Delta p(L) - \Delta p(z)$]. From this point of view, Bierlein *et al.* gave a correct formulation,[27] and similar approaches in an intuitive way were applied in Refs. [9] and [10].

In a generalized case of N pair twin-crystals as that in Ref. [12], the phase mismatch $\Delta p(z)$ incurred by angular detune is periodically valued, i.e., $\Delta k_1 z_1$, $\Delta k_1 l_1 + \Delta k_1 z_2$, $\Delta k_1 z_3$, $\Delta k_1 l_1 + \Delta k_1 z_3$, ..., in an

approximation Δk_0, φ_0=0. Here, $z_{3,4}$ are the relative coordinates like $z_{1,2}$. The final harmonic intensity then is $I_2 \propto (2N\sigma l_1)^2 \mathrm{sinc}^2(\varphi_1)$, which does escape from the inter-plate pulse interference. The engineering errors in the fabrication of WOC structures mostly account for the experimental deviation in Ref. [13], which requires a finer experiment to check. It is clear that the inter-plate pulse interference actually lies in the distribution of phase mismatch among plate pairs. Thus, there is a generalized compensating condition $\Delta p(L)$=0. If φ_0', φ_0 have to be considered, the two crystals can then be slightly tilted to make $\delta k_m = \Delta k_m(\delta\theta = 0) \neq 0$ $(m = 1, 2)$, where the phase mismatch in a single plate should be far less than π, such that $\Delta p(L)$=0 holds for small $\delta\theta$.

4. Exemplification in a passive case

There are many nonlinear crystals in the infrared region, so it is viable to construct an active PMCC at a longer wavelength over 1 μm, as shown in Appendix. However, applications in the visible range are impossible because of the absence of available crystals. Thus one has to go back to the passive WOC method and look for potential crystals of negative δu, which ought to possess a large enough birefringence, transparent in the UV spectral region. Fortunately, BBO itself, α-BBO[31] and calcite come to the rescue. These negative uniaxial crystals have minimal retracting wavelengths at $\theta = 90°$, as shown in Fig. 6(b). Especially for calcite, it can almost compensate for the GVMM in all of the phase-matching ranges of BBO, Cesium Lithium Borate (CLBO), Potassium Dihydrogen Phosphate (KDP) and even Lithium Borate (LBO) in the visible region.

An exploration to the passive WOC PMCC will be continued in this section, since it demonstrates a more subtle situation that is worthy of note. We consider the SHG of 262.5 nm in a PMCC pumped by 100-fs transform limited laser pulses with λ_1 = 525 nm, from the radiation of SHG in a Yb:glass laser (1050 nm). The GCs here are several 0.167 mm thick BBO plates, just equal to the temporal walk-off length $|\Delta\tau/\delta u_1|$. The phase-matching angle is $\theta = 48.6°$ (δu_1 = 598 fs/mm) with the external acceptance $\Delta\theta \approx 1°$. Calcite has to be chosen to compensate for the GVMM ($\delta u_2 = -242$ fs/mm) at such a short wavelength according to Fig. 6(b), which requires a passing length 0.412 mm at $\theta = 90°$ by Eq. (5). We arrange the normal direction of the CC plates to be along the beam direction to realize a maximal angular acceptance, as will be explained below. The small GVMM induced by anti-reflective and protective coatings is neglected. The fundamental pulses in air are assumed to be a form of the parallel Gaussian beam with a Gaussian temporal shape, i.e.,

$$A^{(1)}(r,t) = A_0 \exp\left(-\frac{t^2}{2\tau_0^2} - \frac{r^2}{w_0^2}\right),$$
$$\Delta\tau = 2\tau_0[\ln(2)]^{1/2} \tag{32}$$

with a duration $\Delta\tau$ = 100 fs and a beam waist radius w_0 = 50 μm, which permits overlooking the spatial walk-off (the walk-off length is about 1 mm), and A_0 is the maximal amplitude determined by the pulse energy. Figure 4 demonstrates the angular tuning characteristics where $\delta\theta$ and $\delta\phi$ are the external polar and azimuthal tuning angles, respectively. The curves in Fig. 4(a) are drawn in the θ direction according to the inter-plate pulse interference factor $\cos^2(\Gamma_2) f_N^2(\psi)$. Note that the angular tuning in the azimuthal direction [see Fig. 4(b)] does not cause a mismatch ($D_c \equiv 1$), so the interference factor actually controls the total dephasing process. The function $\mathrm{sinc}^2(\Gamma_1)$ fits D_p well in Fig. 4(c), which clearly validates the cosine approximation of Eq. (20). Figure 4(b) shows that the acceptance in the ϕ direction is so small that it is against one's intuition. This anomaly can be explained by a simple analysis. The variations in Γ_{j2} due to an angular tilt can be expressed as

$$\delta\Gamma_{j2} = (l_2\delta\Delta k_{j2} + \Delta k_{j2}\delta l_2)/2, \tag{33}$$

where Δk_{j2} is the total wave constant mismatch in CC_j, whose value is $2m_j\pi/l_2$ (here $m_j \approx 214$) in a perfect coherence. With a large magnitude of $|\Delta k_{j2}|$, the second term in Eq. (33) is absolutely appreciable. In the θ and ϕ directions, the noncritical (θ, ϕ are near 90° and 0°, respectively) orientation of calcite plates presents insensitive dependence on angular tuning, i.e.,

$$\delta\Gamma_2(\delta\theta) \simeq -0.046(\delta\theta)^2, \tag{34a}$$
$$\delta\Gamma_2(\delta\phi) \simeq 0.072(\delta\phi)^2, \tag{34b}$$

where $\psi = 2\Gamma_2$. Hence, the interference function behaves similarly in the two directions and yields ideal flat tuning tops, as shown in Figs. 4(a) and 4(b). Equations 34(a) and 34(b) make the broad band intra-unit pulse interference factor $\cos^2(\Gamma_2)$ trivial; f_N^2 therefore determines the bandwidth of the azimuthal

tuning. So for a practical PMCC with several units, the interference function can be approximated by

$$\cos^2(\Gamma_2) f_N^2(\psi) \approx f_N^2(\psi)$$

along the two directions.

It can be seen in Fig. 4 that the width of the interference factor decreases quite slowly with the unit number N. By the relation $\delta\psi \approx a_1(\delta\theta)^2$ or $\delta\psi \approx a_2(\delta\phi)^2$ ($a_{1,2}$ are constants), the characteristic widths $\bar{\theta}$, $\bar{\phi}$ of f_N^2 can be estimated at the reference position $N\delta\psi = \pi$, which corresponds to the first root of f_N^2. Then

$$\bar{\theta}, \bar{\phi} \propto N^{-1/2}. \tag{35}$$

This relation relaxes the restriction of $\bar{\theta}$ on $\Delta\theta$ even with a large number of units, e.g., $N = 40$.

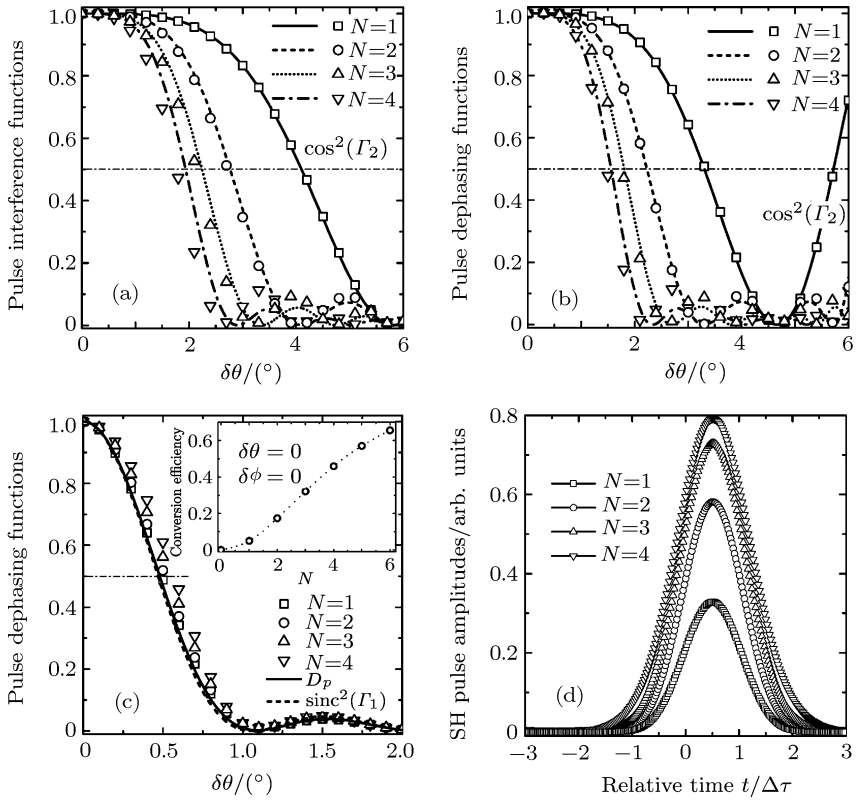


Fig. 4. Pulse interference functions in the directions of θ (a), ϕ (b) by Eq. (19), angular dephasing functions in the θ direction (c) and phase matched harmonic pulse amplitudes (d) are shown in a critical walk-off case $\delta u_1 l_1 = \Delta\tau$ with the results of a depleted simulation (symbolized points) for type *ooe* SHG in a BBO-calcite WOC PMCC with different unit numbers. The inset in (c) gives the maximal conversion efficiencies with different N pumped by 10-nJ pulses.

For a better implementation, a PMCC can be prearranged in a way that all of the odd-ordered CC plates are disposed with an initial tilting angle θ_0 (or ϕ_0), whereas the even-ordered CCs with $-\theta_0$ (or $-\phi_0$). In this case, $\delta\psi \propto (\delta\theta)^2$ or $\propto a_2(\delta\phi)^2$ still holds as before. The thickness fluctuation over different CCs can also be highly suppressed when all of the CC plates are cut from one calcite plate with a high parallelism. [In an active compensation, the second term in Eq. (33) is trivial. So the length tolerance of CC plates is much higher.] Since the total efficiency of the PMCC has a tight dependence on the anti-reflective coating quality, a practical pair number is limited by obtainable engineering precisions and technical levels in a local optical fabrication.

A numerical simulation is taken to verify the model, as is done in a practical case where the pumping pulse energy of 10 nJ is not so small to support the undepleted-pump approximation. The following equations,

$$\frac{\partial A_{j\mu}^{(1)}}{\partial z} + \frac{1}{u_\mu^{(1)}} \frac{\partial A_{j\mu}^{(1)}}{\partial \tau} + \frac{\mathrm{i}\,\beta_\mu^{(1)}}{2} \frac{\partial^2 A_{j\mu}^{(1)}}{\partial \tau^2} = \mathrm{i}\,\sigma_\mu A_{j\mu}^{(2)} A_{j\mu}^{(1)*} \exp(-\mathrm{i}\,\Delta k_{j\mu} z), \tag{36}$$

together with Eq. (1) are numerically solved by the Fourier transform method within 256 sampling time

points and 40 radial spatial points. Numerical results imply that the pulse broadening by the group-velocity dispersion is inessential. A PMCC with N=4 only brings a 16% pulse width increment [see Fig. 4(d)] which does not ruin the chirp-free assumption. The numerical data as shown in Fig. 4 are in good agreement with the model. With an increasing conversion efficiency or number N, the width of the interference function becomes shorter, but the angular bandwidth is wider than the prediction. The simulated angular width changes from 0.96° to 1.14° (a variation of 19%).

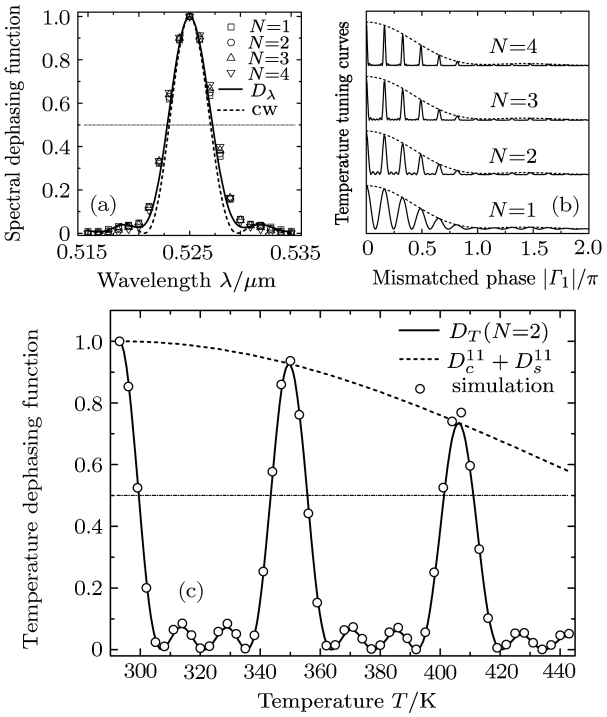


Fig. 5. Pulse spectral (a) and temperature (b) dephasing functions and a numerical simulation to the thermal dephasing process with N=2 (c). The "cw" in (a) means the spectral tuning function $\mathrm{sinc}^2(\Gamma_1)$ given by cw pumping.

The nonlinear phase shift and the consecutively depleted pumping in a fundamental pulse train weakly change the tuning processes, which ultimately contribute to this bandwidth stretching. Simulations are also carried out for spectral and temperature tuning processes, as shown in Fig. 5. As estimated, the spectral dephasing curve, where $D_\lambda = D_c^{11} + D_s^{11}$, demonstrates a main tuning lobe with weak side wings. The width of the main lobe slowly varies with conversion efficiency (or N) from 4.5 nm to 5 nm. However, a strong interference effect is witnessed in the temperature tuning process where $\Gamma_2 = 5.11\Gamma_1$ (the thermo-optic coefficients of calcite come from an extrapolation of the known data in Ref. [32]). The function $f_{2N}^2(\Gamma_1 + \Gamma_2)$ actually governs the temperature bandwidth, which decreases approximately with N as $\Delta T \propto 1/N$. The smallness of the temperature bandwidth is associated with the high thermal sensitivity of the birefringence of calcite.

5. Conclusion

In summary, we investigated a passive four-platelet WOC PMCC together with a proposed active structure for the SHG of low power ultrashort pulses (nJ level). The overall performance of the PMCC depends on the confinement (by compensation) to the spatiotemporal walk-off and to the phase mismatch induced by a detune. The PMCC demonstrates ideal $2N$ times broadened angular and spectral bandwidths, and shows a slowly varying angular bandwidth in proportion to $N^{-1/2}$ in the azimuthal direction. The proposed active WOC method features in efficiency, angular (ϕ) bandwidth and length tolerance, but has a shorter applicable spectral range. A simulation in the depletion case confirms that the variations in dephasing curves are inessential at the efficiencies less than 50% with which the harmonic amplitudes have no evident distortion. A historic controversy is reviewed and it is found that the dispute originates from the phase mismatch term, which confirms that the twin-crystal configuration is out of the inter-plate pulse interference in a perfect compensation case. If the BBO crystal is chosen as a CC, the new PMCC will have similar properties of sensitivity to the three tunable parameters, which generalizes the exemplification. Obviously, the scheme proposed here is easy to apply to the fourth harmonic generation with a cascaded frequency doubling process. With the idea of the polarization rotating method,[24] it can even be used for the third harmonic generation through the SHG and sum frequency generation process (the PMCC will be more complex). However, only amplified ultrashort pulses (not seed pulses) are qualified for an effective frequency tripling via a $\chi^{(3)}$ interaction. Though complicated field dynamics invoked by higher order dispersions, self-phase modulation etc. steps in, a realization of the WOC two-platelet structure in this case, if it is in demand, is quite feasible. A $\chi^{(3)}$ PMCC with more generating crystals is a challenging task that requires a finer design with the help of available compensating elements and possibly needs some pulse shaping devices.

However, a PMCC has to suffer engineering and aligning errors in practice. A pilot study shows that

an inexact configuration will blur and narrow the dephasing peaks to some extent. Detailed results will be presented elsewhere.

Appendix: Active WOC PMCC

The mechanism of active WOC arrangement can be well understood by the retracting points of phase-matching curves. Figure 6(a) demonstrates the phase-matching curves of type I SHG in BBO, CLBO and KDP, the commonly used crystals in the visible and near UV region. The inverse of GVMM in some related crystals is illustrated in Fig. 6(b). The refractive indices used here are from Refs. [33] and [34]. On the phase-matching condition, there are two identities (subscripts are omitted),

$$\frac{\mathrm{d}\theta_m}{\mathrm{d}\lambda_1} = -\frac{\partial\Delta k}{\partial\lambda_1}\left(\frac{\partial\Delta k}{\partial\theta_m}\right)^{-1},$$
$$\frac{\partial\Delta k}{\partial\lambda_1} = \frac{4\pi c\delta u}{{\lambda_1}^2}, \qquad \text{(A1)}$$

where θ_m is the phase-matching angle. Evidently, the equation $\mathrm{d}\theta_m/\mathrm{d}\lambda_1$=0 results in δu=0, at which an angular retracting point exists.[14] The Δu (see the caption of Fig. 6) then has negative and positive values on the left and right of a retracting point, respectively. BBO has a retracting wavelength 1.53 μm, CLBO 1.33 μm and KDP 1.03 μm. So in this range, the shadowed spectral region in Fig. 6(a), the crystal pairs of KDP–BBO, KDP–CLBO and CLBO–BBO are able to be programmed as active PMCCs by Eq. (5).

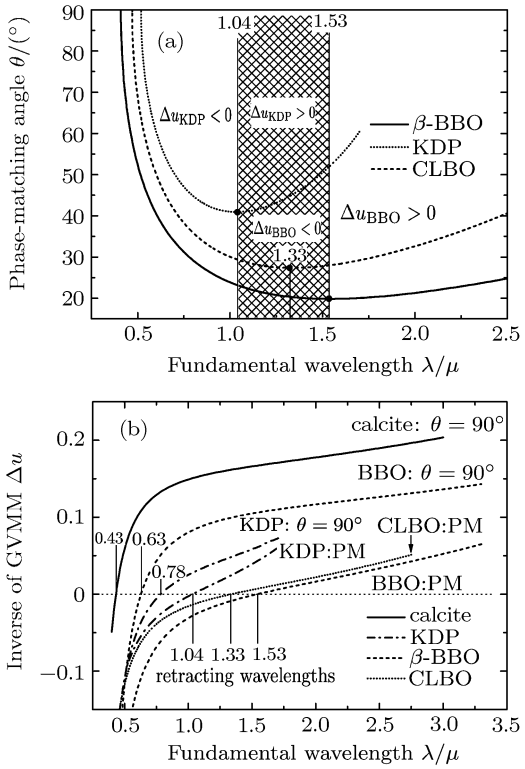


Fig. 6. Phase-matching diagrams of the type *ooe* SHG in β-BBO, CLBO and KDP crystals (a) and the inverses of GVMM (denoted by $\Delta u = -c\delta u$ with the light speed c) of above crystals (b) at 90°, where they have minimal retracting wavelengths, and at their PM angles except calcite.

References

[1] Zeng H P, Wu J, Xu H, Wu K and Wu E 2004 *Phys. Rev. Lett.* **92** 143903

[2] Zeng H P, Wu J, Xu H and Wu K 2006 *Phys. Rev. Lett.* **96** 083902

[3] Lie W Q, Wu J, Cai H and Zeng H P 2009 *Opt. Lett.* **34** 166

[4] Wu G, Li W X, Wu E and Zeng H P 2010 *Opt. Express* **18** 1000

[5] Boyd G D, Ashkin A, Dziedzie J M and Kleinman D A 1965 *Phys. Rev.* A **137** 1305

[6] Kleinman D A, Ashkin A and Boyd G D 1966 *Phys. Rev.* **145** 338

[7] Akhmanov S A, Chirkin A S, Drabovich K N, Kovrigin A I, Khokhlov R V and Sukhorukov A P 1968 *IEEE J. Quantum Electron.* **4** 598

[8] Yanagawa T and Samanta L K 1991 *J. Phys.: Condens. Matter* **3** 7421

[9] Zondy J J, Abed M and Khodja S 1994 *J. Opt. Soc. Am.* B **11** 2368

[10] Smith A V, Armstrong D J and Alford W J 1998 *J. Opt. Soc. Am.* B **15** 122

[11] Gehr R J, Kimmel M W and Smith A V 1998 *Opt. Lett.* **23** 1298

[12] Zondy J J, Bonnin C and Lupinski D 2003 *J. Opt. Soc. Am.* B **20** 1675

[13] Zondy J J, Kolker D, Bonnin C and Lupinski D 2003 *J. Opt. Soc. Am.* B **20** 1695

[14] Webb M S, Eimerl D and Velsko S P 1992 *J. Opt. Soc. Am.* B **9** 1118

[15] Martínez O E 1989 *IEEE J. Quantum Electron.* **25** 2464

[16] Szabo G and Bor Z 1990 *Appl. Phys.* B **50** 51

[17] Danielius R, Piskarskas A, Trapani P Di, Andreoni A, Solcia C and Foggi P 1996 *Opt. Lett.* **21** 973

[18] Smith A V 2001 *Opt. Lett.* **26** 719

[19] Ma J, Zhang R B, Zhang W L and Wang Q Y 2005 *Acta Phys. Sin.* **54** 2745 (in Chinese)

[20] Schober A M, Charbonneau-Lefort M and Fejer M M 2005 *J. Opt. Soc. Am.* B **22** 1699

[21] Huang J, Kurz J R, Langrock C, Schober A M and Fejer M M 2004 *Opt. Lett.* **29** 2482

[22] Fülöp J A, Kovács A P and Bor Z 2001 *Opt. Commun.* **188** 365

[23] Sapaev U K and Assanto G 2007 *Opt. Lett.* **32** 2921

[24] Huang J J, Chang Y Q, Sen T and Yang Y Q 2008 *Opt. Commun.* **281** 5244

[25] Wang Y L, Zhou X G, Wu H and Ding L E 2009 *Chin. Phys.* B **18** 4308

[26] Fève J P, Zondy J J, Boulanger B, Bonnenberger R, Cabirol X, Ménaert B and Marnier G 1999 *Opt. Commun.* **161** 359

[27] Bierlein J D, Laubacher D B and Brown J B 1990 *Appl. Phys. Lett.* **56** 1725

[28] Zondy J J 1995 *Opt. Commun.* **119** 320

[29] Pack M V, Armstrong D J, Smith A V and Amiet M E 2003 *Opt. Commun.* **221** 211

[30] Brown M 1998 *Opt. Lett.* **23** 1591

[31] Zhou G Q, Xu J, Chen X D, Chen W, Xu K, Li H J and Gan F X 2001 *Chinese Journal of Lasers* **26** 320 (in Chinese)

[32] Bass M, Stryland E W V, Williams D R and Wolfe W L 1995 *Handbook of Optics: Devices, Measurements and Properties* Vol. II (New York: McGraw-Hill Inc.) pp. 33, 56

[33] Nikogosyan D N 2005 *Nonlinear Optical Crystals: A Complete Survey* (New York: Springer Science+Business Media, Inc.) pp. 5, 115, 154

[34] Ghosh G 1999 *Opt. Commun.* **163** 95